Original Article

Lanthanum plumbide as a new neutron multiplier material

Ramil Gaisin [a,*], *Pavel Pereslavtsev* [a], *Siegfried Baumgaertner* [a],
Klaus Seemann [a], *Elvina Gaisina* [a], *Vladimir Chakin* [a], *Sergey Udartsev* [b],
Pavel Vladimirov [a], *Bronislava Gorr* [a]

[a] *Karlsruhe Institute of Technology, Hermann-von-Helmholtz-Platz 1, Eggenstein-Leopoldshafen 76344, Germany*
[b] *Ulba Metallurgical Plant, Abay Avenue 102, Ust-Kamenogorsk 070005, Kazakhstan*

ARTICLE INFO

ABSTRACT

A new neutron multiplier based on lanthanum plumbide $LaPb_3$ was produced using two different casting methods. The argon-arc melted material consists of $LaPb_3$ dendrites between grains of $LaPb_2$ phase of approximately equal volume fraction. The induction melted material is composed primarily of large $LaPb_3$ grains, about 80 μm in size. Corrosion testing at 20 and 300 °C in air revealed the rapid degradation of $LaPb_3$ without the formation of a protective passivation layer. The corrosion process results in significant volumetric expansion accompanied by cracking. When $LaPb_3$ is exposed to air at 500 °C, pure lead as a corrosion product melts to form layers protecting against rapid corrosion. $LaPb_3$ showed low (113—193 MPa), but sufficient strength for functional use in the temperature range of 20 —500 °C.

1. Introduction

One of the essential challenges within a framework of the breeder blankets development for the future DEMO fusion facility is an elaboration of such blankets designs that can potentially meet the basic system requirements for tritium breeding capacity, energy deposition, and safety features [1]. The first challenge is producing more than one tritium per neutron from the plasma source ensuring a margin sufficient to take into account tritium losses in the fuel cycle. Due to the natural loss of neutrons in the blanket structure, the tritium breeding would be always below unity unless a so-called neutron multiplier is used to compensate for this effect [2].

A neutron multiplier is a material that should have 1) a high atomic density (i.e. a metal or metal compound) and 2) a sufficiently high neutron multiplication cross section (n,2n) in the energy range relevant for fusion applications. Such a metal inherently absorbs neutrons due to the (n,γ) neutron capture process. Therefore, the neutron multiplier should also have as low as possible parasitic neutron capture cross section below 14 MeV, and especially at low neutron energies. In the framework of the analyses performed in Ref. [3], two metals having most suitable physical properties for use in breeder blankets as the neutron multiplier were identified: beryllium and lead.

The use of these metals in the breeder blanket has its *pros* and *cons* that can impact the DEMO blanket technology [1,4].

Beryllium has the lowest (n,γ) and sufficiently high (n,2n) (with a threshold of ≈1.85 MeV) reaction rates in the typical DEMO blanket neutron spectrum. On the other hand, lead has the highest (n,2n) (with a threshold of ≈8.2 MeV) and the low neutron capture reaction rates. The atomic density of Be is about four times higher than that of lead, making Be a highly efficient neutron multiplier compared to Pb. Due to its relatively high melting point of 1287 °C, Be can be used in the solid state in DEMO blankets [5], while lead is mostly used in liquid form due to its low melting point of 327 °C [6]. The main disadvantages of the Be neutron multiplier are its considerable cost related to its limited natural reserves and the fact that it presents a health hazard for sensitive persons on inhalation of small particles, which can occur mainly during mining, processing or conversion into metal alloys and scrap processing [7]. In contrast, lead used as a neutron multiplier is widely available and inexpensive. The primary concerns when using lead in a breeder blanket are liquid metal corrosion of the steel structure and the risk of partial solidification in stagnant zones of the blanket [1].

The cost of fusion energy and facilities is a critical factor that can impact its public acceptance. To reduce costs, researchers are investigating alternative neutron multiplier solutions based on lead, such as solid compounds [8]. These compounds should have a melting point of at least 500 °C to ensure reliable operation of the blanket steel structure. One promising solution would be an intermetallic alloy of Be and Pb, which forms an ordered solid-state compound. This alloy would have a low Be content and combine the most attractive properties of each element, making it highly effective as a neutron multiplier, solid and inexpensive. To explore this possibility, the authors conducted preliminary tests to combine lead with beryllium. However, these tests did not result in the formation of a solid alloy, as lead and beryllium in the liquid state are insoluble and do not form compounds during crystallization. The phase diagram of the Pb—Be system appears to be similar to that of the Sn—Be system [7]. Attempts with ternary systems (Be—Pb—Ti and Be—Ti—Zr), containing a high amount of lead and small amounts of beryllium and the third element, were also unsuccessful.

One of the most promising solid compounds based on lead that could potentially be used in the breeder blanket is LaPb$_3$ [3]. With a melting point above 1100 °C, this compound could be used in the form of solid blocks filling the interior space of the blanket. The tritium breeding performance of the breeder blanket with this neutron multiplier was found to be comparable to that of blanket filled with pure liquid lead [1]. In terms of cost, rare earth lanthanum is widely used in the manufacture of conventional lighters and catalysts and its use would only slightly increase the final costs. The breeder blanket filled with the LaPb$_3$ blocks would drastically reduce the investments in the DEMO, compared to the blanket with the solid Be-based neutron multiplier [3]. The replacement of liquid lead with the LaPb$_3$ blocks enables the blanket layout with highly reduced corrosion problems and without a liquid lead loop leading to a very compact and inexpensive DEMO design.

While there have been a few studies on the properties of LaPb$_3$, including thermal [9—11], electromagnetic properties [10,12,13], and electronic structures [11,12], there is still much

that needs to be understood about this material if it is to be used as a neutron multiplier in a breeder blanket. One of the key factors to consider is whether the material will retain its shape at temperatures of up to 500 °C, without softening or cracking. Additionally, it is important that the material exhibits good corrosion resistance in air and water, to prevent corrosion during manufacturing and assembly of the breeder blanket. To better understand these properties, a study has been conducted on the melting of ingots of lanthanum plumbide, as well as on its structure and mechanical and corrosion properties. By examining these factors in detail, it may be possible to determine whether LaPb$_3$ is a viable option for use as a neutron multiplier in a breeder blanket, and what steps may be needed to ensure its reliability and safety in this application.

2. Materials and experimental techniques

Granules of pure lead (+30 mesh, 99.99%, Alfa Aesar) and pieces of pure lanthanum (99.9%, Alfa Aesar) were taken as starting materials. The pieces of lanthanum were stored in oil and washed in acetone before melting. Ingots of pure lanthanum and lead were preliminarily melted, their surfaces were further ground mechanically to remove an oxide film. The first ingots were obtained by argon-arc melting using an Edmund Bühler AM furnace. The ratio of pure lead and lanthanum in the alloy was Pb-19 wt% La (hereinafter Pb—19La), which corresponds to Pb-25.9 at.% La. The selected composition is close to the target composition of LaPb$_3$ (Pb-25 at.% La) with a slight shift in more lanthanum towards the LaPb$_2$ (Pb-33.3 at.% La) to avoid the formation of a pure lead phase with a low melting point (Fig. 1). When melted, lead and lanthanum react intensely. During melting and 4 remeltings, the mass of the ingot decreased by 12% due to the evaporation of lead (confirmed by chemical analysis of powder). The evaporated lead after melting adhered in the form of a powder to the surface of the chamber (Fig. 2a). The dimensions of the ingots after melting were about Ø40mm × 16 mm (Fig. 2b).

To reduce the evaporation of lead during melting, subsequent ingots were prepared by induction melting. The mitigation or prevention of lead evaporation can be achieved by means of rapid induction melting and intensive mixing with eddy currents, which enable the lead to be more effectively retained within the molten material. Tantalum was experimentally chosen as the material of the crucible, as it does not react with the melt. Melting took place in a laboratory induction furnace installed in a glove box with an argon atmosphere (Fig. 2c). After melting, the liquid was poured into copper molds. Four experimental ingots weighing 200—300 g each were cast (Fig. 2d).

The structure of the alloys was studied using optical (OM) and scanning electron microscopy (SEM). The structure was prepared by grinding and mechanical polishing without the use of water. The elemental analysis of La, Pb and O was carried out with energy-dispersive X-ray spectroscopy (EDS). Electron backscatter diffraction (EBSD) was used to build surface normal-projected inverse pole figure (IPF-Z) orientation maps. Density was measured by the hydrostatic weighing
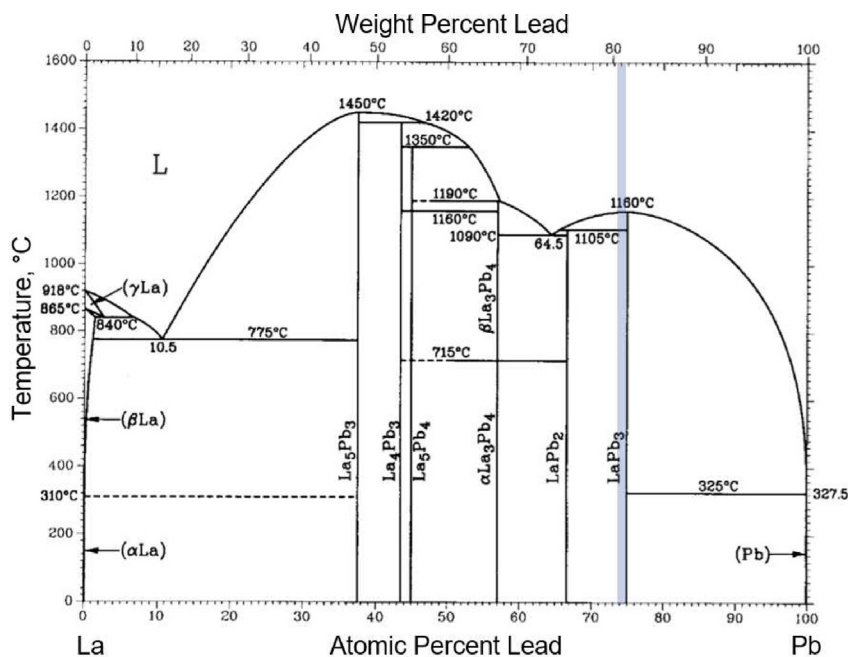
Fig. 1 — La—Pb phase diagram [1]. The blue area indicates the studied composition of Pb—19La (wt.%).

in $C_{14}H_{30}$ liquid medium. Microhardness was measured using indentation forces of 10—2000 gf. X-ray diffraction (XRD) measurements were performed on a Seifert PAD II diffractometer with Cu-K$\alpha_{1/2}$ radiation. Corrosion tests at room temperature were carried out in air at about 40% humidity for about 2100 h. Humidity was monitored with a room hygrometer. Periodically, the sample was weighed and the mass gain

per area was calculated. Corrosion tests at 300 and 500 °C were carried out in air in a resistance furnace for about 30 h. In this case, the humidity could not be controlled and the samples were periodically removed from the furnace to measure the weight gain. Mechanical compression tests were carried out in vacuum at temperatures of 20, 300, and 500 °C on samples of Ø5mm × 6 mm. The initial strain rate was 10^{-3} s^{-1}. After
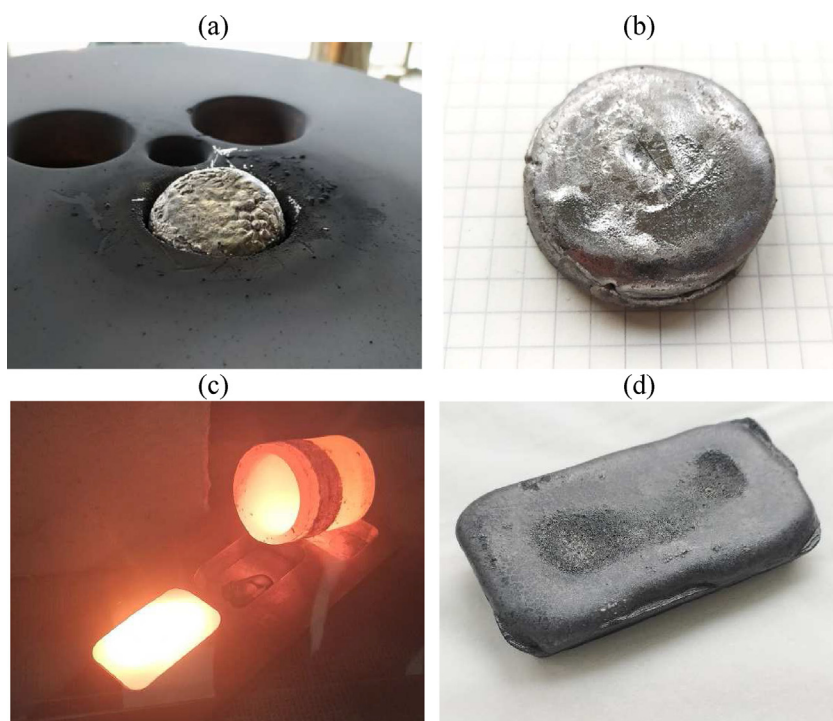

Fig. 2 — (a,c) Casting of Pb—19La alloy and (b,d) the resulting ingots. (a,b) argon arc melting, (c,d) induction melting with pouring into a copper mold.

mechanical tests, the fracture surface of the samples was studied.

3. Results and discussion

3.1. Microstructure

Initially, argon-arc melting was chosen as the simplest way for producing $LaPb_3$ ingots, following the procedure described in Refs. [14,15]. Fig. 2b shows a typical Pb—19La ingot obtained by argon arc melting. There are shrinkage cavities and cracks at the surface, apparently due to rapid cooling during the solidification. The ingot's density of 9.93 g/cm^3 is lower than the calculated from X-ray data density of $LaPb_3$ of 10.713 g/cm^3, as reported in Ref. [15]. Although the ingot had a shiny surface immediately after melting, it tarnished an hour later, possibly due to corrosion in air. Such a fast interaction with air/water vapor was observed previously in Ref. [15]. To decrease the loss of lead from its evaporation, induction melting in a tantalum crucible was chosen as in Refs. [9,10]. Fig. 2d shows an example of a Pb—19La ingot (65 × 38 × 12 mm^3) produced by induction melting. A shrinkage cavity is present at the surface of the ingot without visible cracks. The density of this ingot is much higher and reaches 10.54 g/cm^3. To avoid possible corrosion in air, all alloy ingots were placed in an oil container after melting.

Fig. 3 presents X-ray diffraction patterns of Pb—19La after argon arc melting and induction casting. Since the measurements were carried out in air, the first sample was ground right before the measurement. In the case of the ingot obtained by induction melting, the sample was exposed to air for about 1 h before the measurement. The XRD patterns show main peaks that can be attributed to both $LaPb_3$ and lead, which have very close peaks with a slight shift [15]. These peaks are partly broadened and doubled indicating the presence of both phases at the surface. Based on the density measurement data, the main phase is $LaPb_3$, while pure lead may cover the surface when corroded during the measurement (to be shown below). The diffraction patterns also have strong peaks corresponding to lead oxide and lanthanum hydroxide, especially in the case of the sample exposed to air prior to measurement. It was not possible to confirm the presence of other lanthanum plumbides ($LaPb_2$, La_3Pb_4) using XRD, since their structure has not been described before and, accordingly, there is no XRD data for them [15]. The presence of other lanthanum plumbides may explain the peaks at about 37° (Fig. 3a), which cannot be identified as $LaPb_3$, Pb, or PbO. The same unidentified peak is present in the diffraction pattern of $LaPb_3$ (with shifted composition) in Ref. [14]. XRD studies of Pb—19La after exposure to air showed that even 1 h was enough for $LaPb_3$ to corrode with the formation of phases of lead, lead oxide and lanthanum hydroxide at the surface.

The microstructure of the Pb—19La alloy obtained by the argon-arc melting is shown in Fig. 4a and b. During crystallization, a two-phase dendritic structure was formed with a length of dendrites up to 500 μm and a thickness of about 20 μm. The dendrites are oriented mainly along the direction of heat removal in the ingot. The volume fraction of the phase
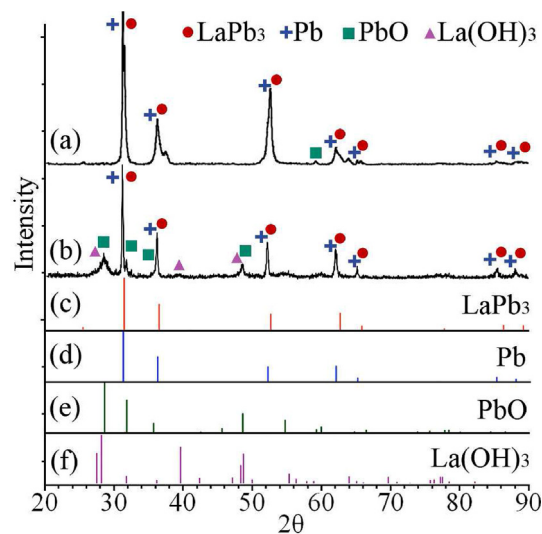

Fig. 3 — X-ray diffraction patterns of Pb—19La obtained by (a) argon arc-melting, (b) induction melting. (a) was polished just before and (b) 1 h before the measurement. The peaks corresponding to (c) $LaPb_3$ (PDF: 03-065-7232), (d) Pb (PDF: 00-004-0686), (e) PbO (PDF: 01-072-0151), and (f) $La(OH)_3$ (ICSD: 239411), used for the analysis, are shown below the diffraction patterns.

corresponding to the dendrite axes is about 53%. EDS analysis (Fig. 5) showed that the two phases differ significantly in chemical composition. The dendritic axes have a composition of 77 Pb—23La (at.%), which is close to the composition of $LaPb_3$. The interdendritic space contains more lanthanum and less lead with the composition of 66 Pb—34La (at.%), which corresponds well to the $LaPb_2$ compound that was not found using XRD because of the lack of corresponding data. The dendrite axes contain a slightly higher oxygen compared to the interdendritic space. The observed two-phase dendritic microstructure could arise upon cooling of the melt with lower lead content (due to evaporation), and, accordingly, the composition shifted towards a higher content of lanthanum. In this case, the $LaPb_3$ phase (dendritic axes) crystallizes first. When the temperature reaches 1105 °C, the $LaPb_2$ phase is formed in the interdendritic space from the liquid and a part of $LaPb_3$ according to the peritectic reaction L + $LaPb_3$ → $LaPb_2$ [15,16].

The microstructure of the sample obtained by induction melting consists of large grains of $LaPb_3$ with an average size of about 80 μm according to EBSD analysis (Fig. 4c and d). A second phase with a volume fraction of about 3% is observed along grain boundaries, at triple junctions, and sometimes inside $LaPb_3$ grains. This phase cannot be identified using EBSD and, therefore, is shaded in black. The distribution of these particles can represent the boundaries of $LaPb_3$ dendrites during crystallization. EDS analysis (Fig. 6) showed that the ratio of Pb and La in $LaPb_3$ is 73 Pb—27La (at.%), while in the second phase 66 Pb—34La (at.%), which can correspond to the $LaPb_2$ phase. In addition to these two phases, the structure contains acicular particles with a lanthanum to oxygen ratio
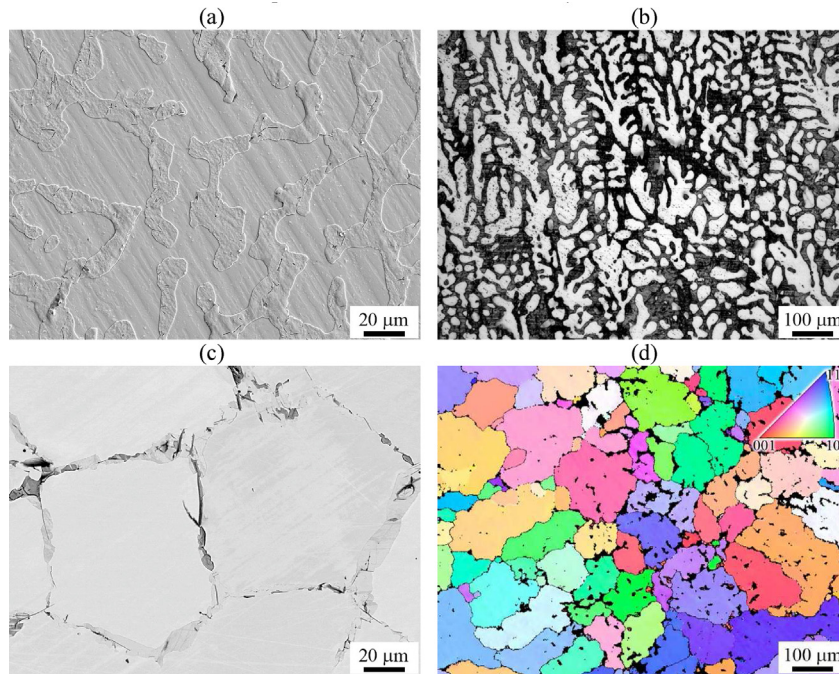
Fig. 4 — Microstructure of Pb—19La obtained by (a,b) argon arc-melting, (c,d) induction melting. (a,c) SEM, (b) OM, (d) EBSD map of LaPb₃ phase. The black and white lines on the EBSD map indicate high- and low-angle grain boundaries, respectively.

of 43La—57O (at.%). These particles can represent the lanthanum oxide La_2O_3 particles. The same particles are observed in the structure of the ingot prepared by argon-arc melting (Fig. 5), but there is no high oxygen content, probably due to the fact that the particles fell out during sample preparation.

In general, the ingots obtained by two methods have similar two-phase structure with $LaPb_3$ dendrites/grains and $LaPb_2$ in the interdendritic space. The use of induction melting prevented a strong evaporation of lead, and therefore the content of the second phase turned out to be much lower. Regarding the use of such materials as the neutron multiplier,
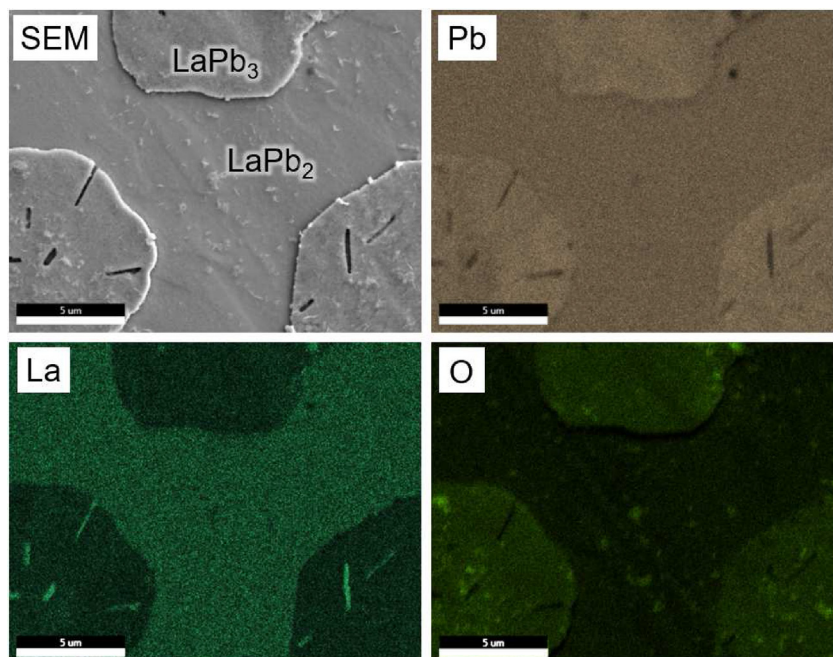
Fig. 5 — SEM image and corresponding EDS maps of Pb—19La obtained by argon arc melting.
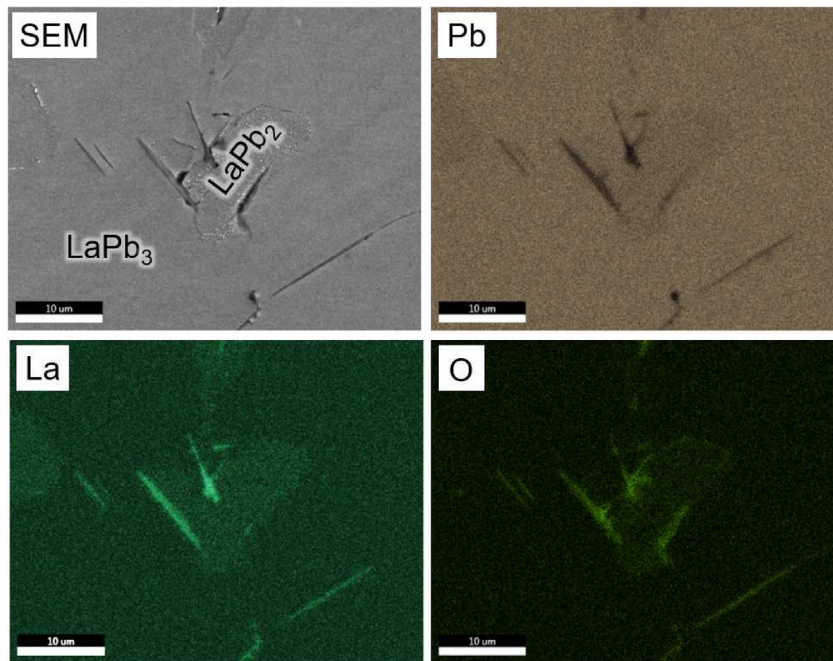
Fig. 6 − SEM image and corresponding EDS maps of Pb−19La obtained by induction melting.

the lead content should be as high as possible. Therefore, only Pb−19La ingots obtained by induction casting containing a minimum amount of the $LaPb_2$ phase were used for further study.
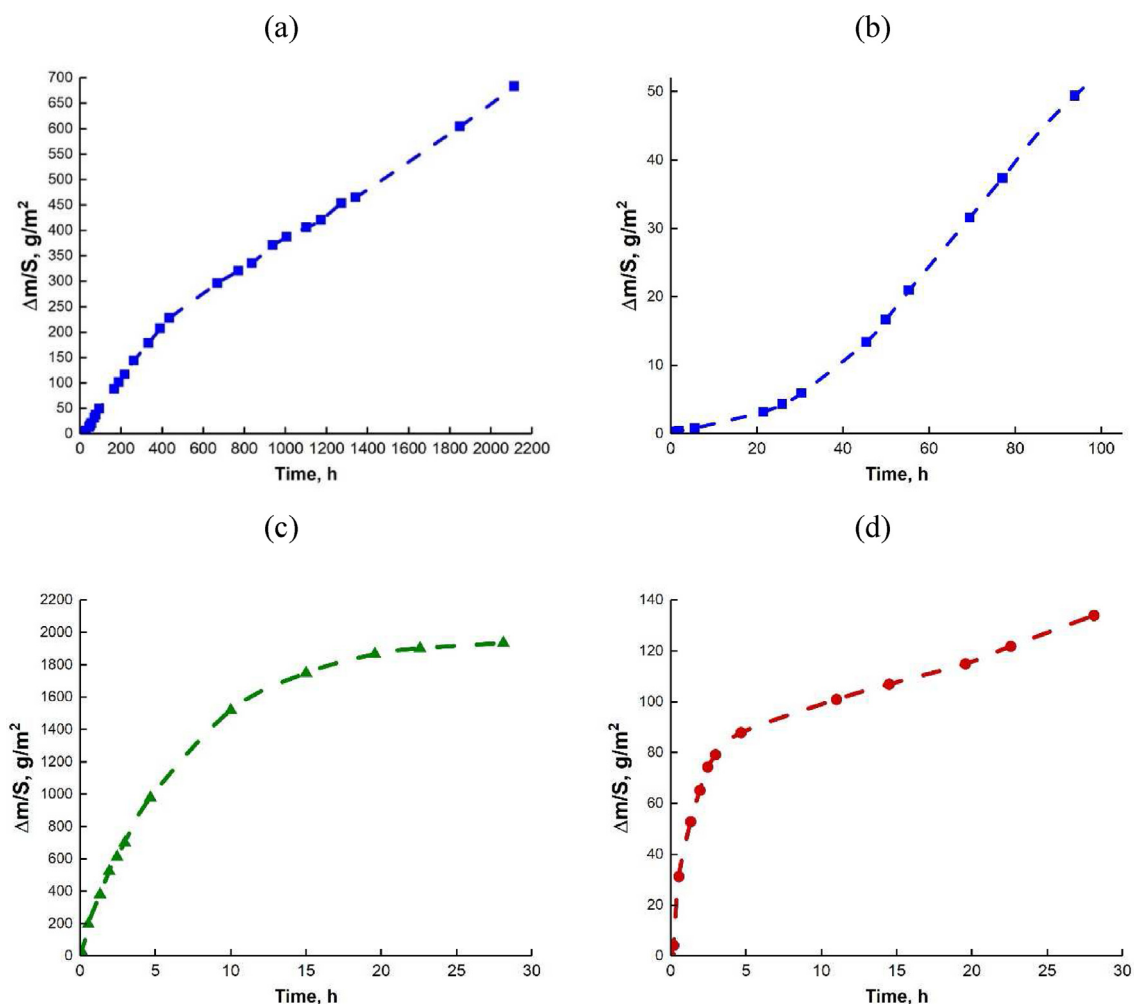
3.2. Corrosion

As already noted, the surface of the first Pb−19La ingot began to tarnish already in the first hours after melting. Therefore, to use this material in the breeder blanket as a neutron multiplier material, it is necessary to apply some technical measures to prevent and suppress corrosion processes. If LaPb3 blocks are accepted as the material for neutron multiplication in the DEMO breeder blanket, no purge gas is preliminarily assumed to remove gaseous products outside the blanket. However, some secure system is anticipated in transient or emergency process in such a breeder blanket to evacuate gaseous products and to protect the equipment. Assuming that such accidents could potentially occur, the LaPb3 blocks could come into contact with air or water released from the cooling system. In order to preliminary check the corrosion resistance, simple experiments were carried out with placing the samples of Pb−19La (produced by induction melting) with a dimension of about $10 \times 10 \times 5$ mm^3 in air (with 40% humidity) or in water at room temperature and in air at 300 and 500 °C.

The kinetic plot for the corrosion of Pb−19La in air at room temperature and about 40% humidity is shown in Fig. 7. Three intervals with different corrosion kinetics can clearly be distinguished. The initial stage of corrosion lasts about 50 h (Fig. 7b) and obeys a parabolic rate law. According to the fitting, the weight gain per area (in g/m^2) can be determined as $\Delta m/s = 0.005\ t^{2.071}$, where t is corrosion duration in h. Both in

the second and in the third stages, the corrosion kinetics obeys the linear rate law. Up to approximately 500 h, a higher corrosion rate, i.e. 0.512 g/m^2/h was detected, while at a later stage, it decelerates yielding a value of only 0.268 g/m^2/h. The lower corrosion rate observed between 500 h and 2100 h can be attributed to the lower diffusion flux of gaseous species to Pb−19La due the formation of an outer scale. A similar experiment was carried out in Ref. [14] where LaPb$_3$ samples were exposed to air at room temperature. The corrosion rate turned out to be much faster and amounted to about 8% weight gain in 20 days. In the present work, the weight gain was about 2% over the same period. Such a difference may be due to the fact that the authors studied not a LaPb$_3$ sample, but of a shifted composition towards higher lanthanum content [14]. Other reasons could be a higher humidity during the experiment and/or a relatively large area of the sample as the geometric dimensions of the samples were not indicated in the study.

The primary factor contributing to the rapid corrosion of Pb−19La at room temperature in air is the presence of lanthanum in its composition, which exhibits a high affinity for oxygen. Lanthanum is well-known to corrode rapidly in air, particularly in the presence of water vapor. According to [17−19], the corrosion rate of lanthanum at 35 °C is 0.33 g/m^2/h and 2.13 g/m^2/h at air humidities of 1% and 75%, respectively. Therefore, it can be inferred that the Pb−19La alloy corrodes in a similar or slightly slower manner (0.268 g/m^2/h) than pure lanthanum metal during the second linear stage of corrosion.

In the case of corrosion tests at a higher temperature of 300 °C, an exceedingly rapid corrosion behavior is observed (Fig. 7c). Within the first 6 h, the weight gain reaches 1000 g/m^2. By the 20−30 h, the rate of corrosion significantly

Fig. 7 – Corrosion kinetic plot of Pb–19La alloy in air: (a) at 20 °C and 40% humidity, (b) an enlarged view of initial corrosion stage in (a), (c) at 300 °C, and (d) at 500 °C.

decreases, and ultimately comes to a halt. The corrosion behavior conforms to an exponential law, with the weight gain per area (in g/m²) being able to be calculated as $\Delta m/s = -1955 \cdot e^{-t/6.655} + 1964$, where t is corrosion duration in h. Contrary to expectation, this behavior is not attributed to the formation of any passivation layer. Instead, it is a result of the consumption of all LaPb₃ during the tests, as elaborated below. Corrosion at 300 °C can be also is associated with a significant volumetric effect that leads to crack opening and rapid corrosion. Although the mechanism of corrosion at 300 °C and room temperature is similar, the process is accelerated at higher temperatures.

Upon increasing the testing temperature to 500 °C (Fig. 7d), corrosion is significantly reduced as compared to the previous temperature of 300 °C. After approximately 20 h of corrosion, the specific weight gain during corrosion at 500 °C was 16 times less than that at 300 °C. At 500 °C, a relatively fast corrosion stage is followed by a linear corrosion stage after roughly 5 h. The corrosion rate during this linear stage is measured at 2.007 g/m²/h, which is approximately 7.5 times faster than at room temperature. It is evident that at 500 °C,

there exists a protective mechanism that inhibits very rapid corrosion, compared to 300 °C.

Fig. 8 shows the microstructure of the sample surface after exposure to air for different times. EDS analysis showed (not presented in the work) that after 8 h in air, particles of pure lead about 1 μm in length and about 200 nm in thickness appeared on the surface. The formation of lead particles were detected to be faster near grain boundaries, apparently due to accelerated grain boundary diffusion. These lead particles merge and protrude from the grain boundaries forming ramified structure. In Ref. [14] a very similar corrosion was observed, where these particles were denoted as lead nodules and whiskers. The formation of whiskers even at room temperature is a well-known concern in electronic applications. However, the mechanism of whiskers growth is not properly understood. Jackson and Crandall postulated in their review that whisker growth can results from intrinsic or extrinsic stresses in the growing outer layer [20]. Moreover, it is suggested that the whisker growth accelerates (i) at increasing temperature and (ii) in humid atmosphere [20,21]. It can therefore be assumed that gaseous species such as oxygen
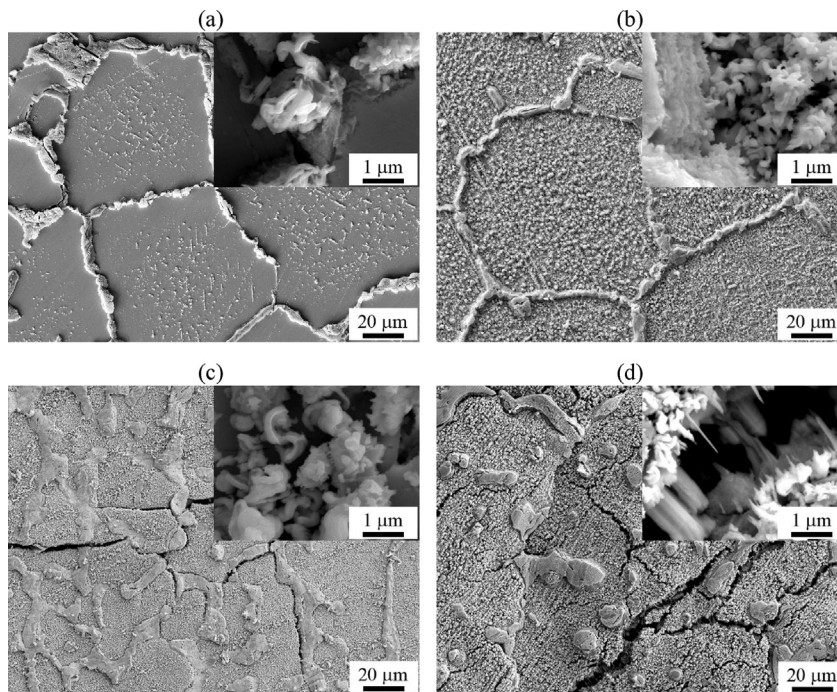
Fig. 8 – Surface microstructure of the Pb–19La sample after exposure to air for (a) 5 h, (b) 1 day, (c) 8 days, (d) 56 days.

and water vapor can diffuse into material causing severe stresses and giving rise to the formation of nodules/whiskers on Pb–19La. In Ref. [8], it was proposed that whiskers are formed as a result of the corrosion of LaPb₃, through the following reaction:

$$LaPb_3 + 3H_2O \rightarrow La(OH)_3 + 3\,Pb + 3H \quad (1)$$
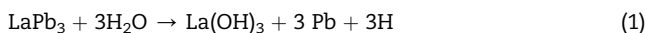
After 1 day (Fig. 8b), the entire surface of the sample was covered with often curved nodules of pure lead, the grain boundaries with lead nodules became thicker. After 8 days (Fig. 8c), cracks developed along the grain boundaries became visible, likely due to the strong volumetric expansion due to corrosion. After 56 days of corrosion (Fig. 8d), cracks were found everywhere at the surface. Cracks often propagate across the former grain boundaries.

After 88 days of corrosion, the sample was embedded into resin and afterwards it was ground to half the height. A corrosion layer of 1000–1500 μm in thickness was formed. The cross-section micrograph and the corresponding EDS maps are presented in Fig. 9. It shows the propagation of corrosion in the sample, starting from the edge of the sample on the right to the centre of the sample on the left. EDS maps of oxygen distribution shows higher oxygen content along the grain boundaries indicating that the corrosion process is governed by oxygen inward diffusion causing severe internal oxidation. Fig. 9 clearly shows that La oxidizes preferably due to its high affinity to oxygen, while Pb – a thermodynamically much nobler element – exhibits a much higher resistance as a lot of unoxidized Pb islands are still visible in the zone of internal oxidation. The reaction products formed between grains during corrosion have very likely a larger volume than

LaPb₃, this results in tensile stresses and cracking, providing an easy path for air to enter the sample. Cracks run not only along the grain boundaries, but also inside the grain itself, causing further corrosion within the grain (Fig. 10a). Fig. 10b and EDS maps in Fig. 9 show alternating layers of pure lead and layers with a high content of lanthanum and oxygen. Thus, a dense passivation layer was not formed at the surface of the sample, which could protect the material from further corrosion.

Knowing the density of the reaction products in (1), the volumetric effect of the corrosion reaction can be assessed to explain the cracking. The volume of the mixture of pure lead and lanthanum hydroxide exceeds the volume of lanthanum plumbide by 39.7%. Such increase of the sample volume could explain the intensive cracking propagation.

Small peaks of La(OH)₃ were also found in the diffraction pattern of the sample, which was exposed to air for 1 h (Fig. 3b). Therefore, the main driving factor for corrosion appears to be humidity rather than oxygen in the air. To test this assumption, another sample of the Pb–19La alloy was placed in water (Fig. 11). The very intensive chemical reaction was observed resulting in a brake of the sample into pieces in 2 h. Such fast corrosion process prevented further measurement of the weight gain in the sample. During the reaction, the temperature increase was found accompanied by a hydrogen release. After about one day keeping the sample in water, it completely corroded and crashed into fragments (Fig. 11b).

Fig. 12 illustrates the appearance of the Pb–19La samples after exposure to air at elevated temperatures of 300 and 500 °C for durations of 1 and 30 h. At 300 °C, already after 1 h, rapid corrosion develops so that the reaction products form a layer that repeats the faces of the initial shape of the sample
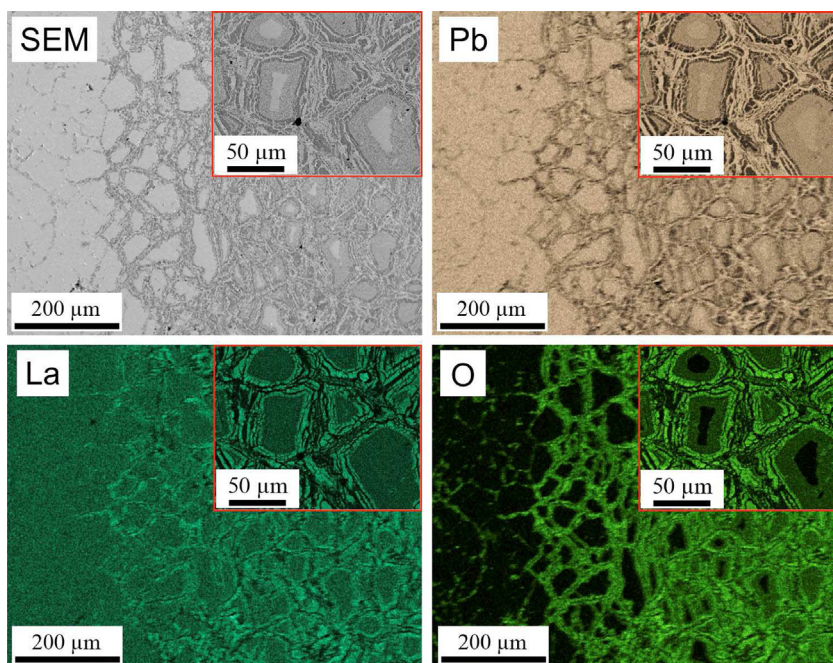
Fig. 9 — SEM image and corresponding EDS maps of Pb—19La sample after exposure to air for 88 days. The edge of the sample is on the right.

(Fig. 12a). After about 30 h of corrosion, the sample was completely consumed, with all $LaPb_3$ subject to corrosion (Fig. 12b). This phenomenon explains the observed reduction and cessation of corrosion after 20—30 h, as demonstrated in Fig. 7c.

Regarding the corrosion behavior of $LaPb_3$ at 500 °C, the most notable feature is the formation of pure lead droplets on the sample surface immediately upon corrosion initiation (Fig. 12c—d). Subsequent chemical analysis confirmed the composition of droplets as pure lead. These droplets can accumulate on the surface of the sample and coalesce into larger droplets. However, with extended corrosion time, no substantial growth or formation of new lead droplets is observed, and the initial droplets eventually detach from the sample surface due to periodic transfer from the furnace to

the balance. The shape of the sample remained unchanged after 30 h.

To elucidate the corrosion protection mechanism at 500 °C, the Pb—19La sample was embedded in an electroconductive resin and polished to half its height. Fig. 13 depicts the microstructure and corresponding EDS maps of the sample after exposure to air at 500 °C for 30 h. A corrosion layer measuring up to 450 μm in thickness was observed on the $LaPb_3$ surface. Notably, this corrosion layer exhibited reduced electrical conductivity compared to layer formed at 20°C, resulting in a brighter appearance in the SEM photograph. Analysis of the corrosion layer revealed the presence of a phase containing lanthanum and oxygen in a near 41La—59O ratio (at.%) throughout its entire thickness. This phase may correspond to the formation of lanthanum oxide (La_2O_3)
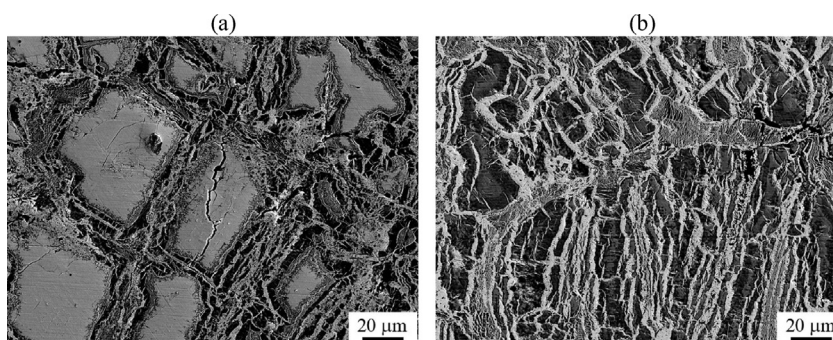
Fig. 10 — Pb—19La sample after exposure to air for 88 days: (a) further formation of new cracks inside the grains, (b) alternating layers of high lead (bright) or high lanthanum and oxygen (dark).

Table 1 − Mechanical properties of Pb−19La alloy after compression tests at room and elevated temperatures.

T, °C	ε, %	$\sigma_{0.2}$, MPa	σ_{max}, MPa
20	12.8 ± 0.8	138 ± 9	193 ± 15
300	11.9 ± 1.3	123 ± 10	163 ± 10
500	>50	95 ± 17	113 ± 25

rather than lanthanum hydroxide, as the latter decomposes into La_2O_3 and water upon heating above 300 °C.

Within the entire corrosion layer, thinner layers up to 50 μm in thickness can be found, containing lead and negligible amounts of oxygen or lanthanum. These layers are most likely comprised of pure lead, which forms during the corrosion of $LaPb_3$, alongside lanthanum oxide/hydroxide. At 500 °C, the lead, being in a liquid state, could come out on the surface of the sample and form droplets. As the corrosion time increased and the thickness of the corrosion layer grew, the lead became trapped within the layer, forming a layer of liquid lead therein. Evidently, diffusion of oxygen through the layer

of liquid lead and into the interior of the material is much slower than through cracks, which are constantly formed due to the strong volume effect during corrosion at 20 and 300 °C. This presents opportunities for protecting $LaPb_3$ from corrosion, particularly if utilized within a breeder blanket. Continued investigation into the corrosion behavior of $LaPb_3$ is ongoing. The observed phenomenon may also theoretically be applicable to corrosion protection of other materials. Crucially, the formation of a liquid phase during corrosion at operating temperatures, capable of filling pores and cracks, may prevent the rapid penetration of the corrosive agent deep into the material. Even if this protective layer is damaged, further corrosion may contribute to the self-healing of the surface.

The Pb−19La alloy exhibits moderate resistance to oxidation in air with 40% humidity at room temperature and completely fails after a few hours in water. This behavior can primarily be attributed to the peculiarity of the environment, i.e., humidity or water. Pure lead, formed in the samples due to corrosion, could cause malfunction of the breeder blanket
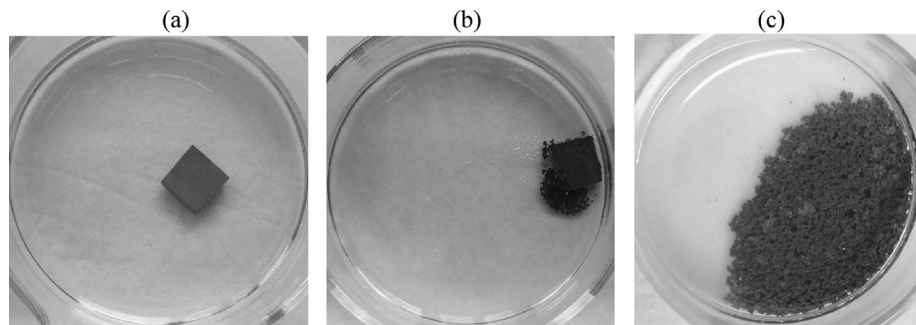
Fig. 11 − Pb−19La sample corrosion in water at 20 °C after (a) 10 min, (b) 4 h, (c) 1 day.
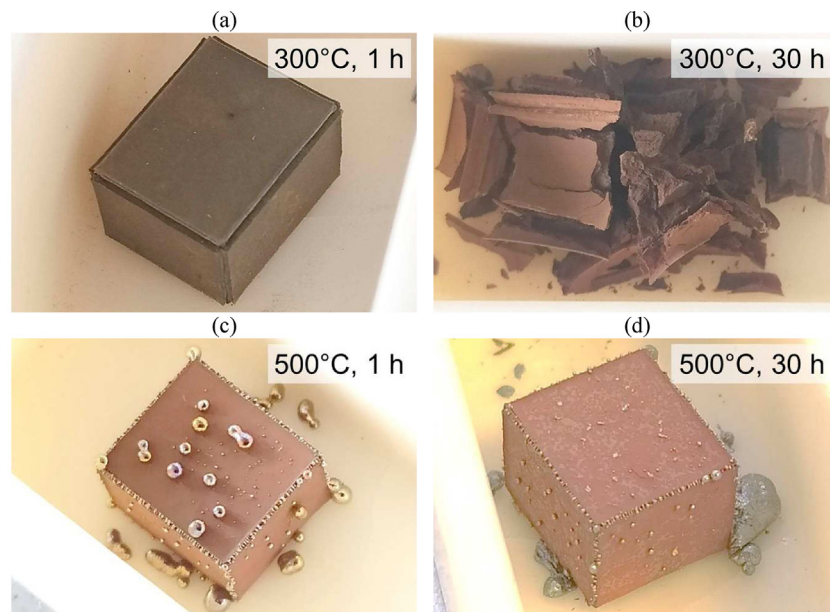
Fig. 12 − Appearance of Pb−19La samples after corrosion tests at (a,b) 300 and (c,d) 500 °C in air for (a,c) 1 and (b,d) 30 h.
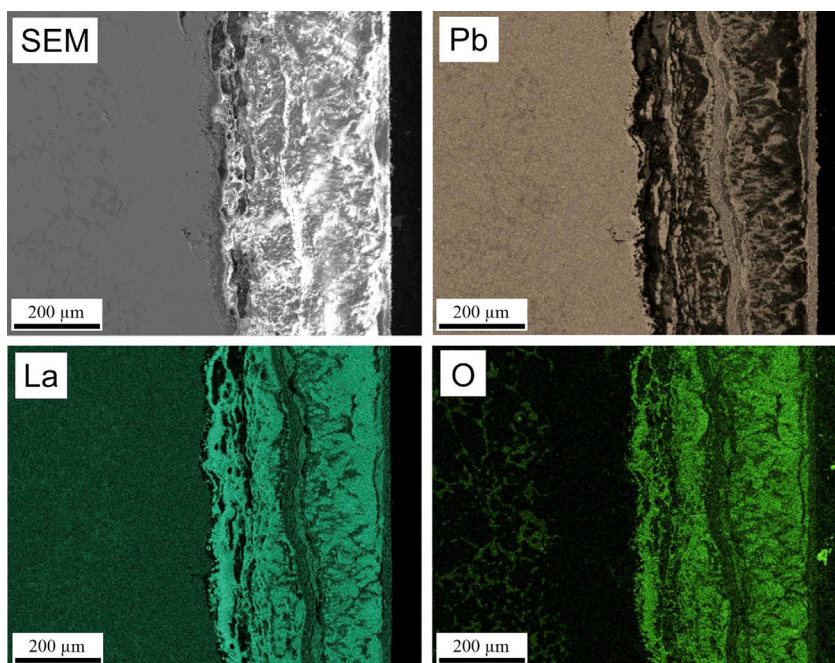
Fig. 13 — SEM image and corresponding EDS maps of Pb—19La sample after exposure to air at 500 °C for about 30 h. The edge of the sample is on the right.

during reactor operation due to its melting at operating temperatures. On the other hand, at such high temperatures, pure lead can form a liquid layer of lead within the corrosion layer, thereby mitigating against accelerated corrosion. In the practical use of Pb—19La blocks, the blocks must be handled in a protective atmosphere to exclude corrosion processes. A realistic approach to protect the blocks from contact with water or water vapor in the blanket could be a use of a protective casing made, for example, of steel.

3.3. Mechanical properties

The hardness measurements of Pb—19La alloy samples obtained by induction melting were conducted immediately
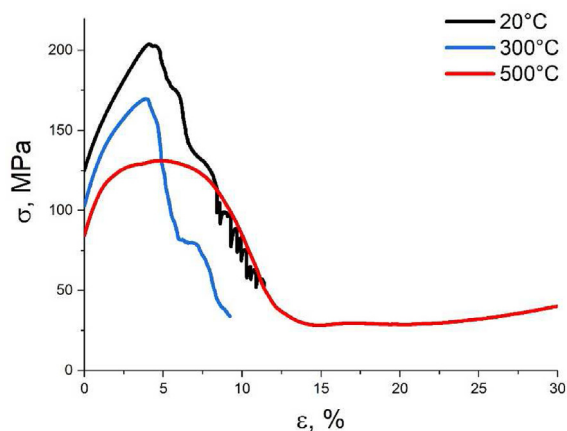
Fig. 14 — Typical compressive stress-strain curves of Pb—19La obtained by induction melting.

after grinding. Indentation forces ranging from 10 g to 2 kg were applied, and $LaPb_3$ showed a consistent hardness of 100 ± 5 HV regardless of the force applied. To measure the hardness of the $LaPb_2$ phase formed along the grain boundaries, a lower indentation force of 10—50 gf was used due to the smaller particle size. $LaPb_2$ had a slightly lower hardness of 70 ± 10 HV. In Ref. [7], the hardness of $LaPb_3$ was reported to be slightly higher (116.6 HV) possibly due to differences in manufacturing methods and lead content.

Table 1 shows the results of mechanical compression tests. The alloy showed a strength of about 193 MPa at room temperature, which decreases but does not drop sharply to 113 MPa at 500 °C. For comparison, he strength of lead at room temperature is only about 10—20 MPa and decreases significantly at 300 °C (melting point of Pb is 327 °C) [22].

Fig. 14 depicts typical compressive stress-strain curves for Pb—19La specimens tested in vacuum at three different temperatures: 20 °C, 300 °C, and 500 °C. At room temperature and 300 °C, the compression after reaching maximum stress is followed by a sharp decrease in stress, which is associated with crack formation. However, the samples do not rapidly fracture completely because the central volume continues to resist the load until new cracks form. At room temperature, a serrated flow curve is observed after about 7% deformation, indicating an increase in stress (Fig. 14). The Pb—19La samples appeared to be brittle at 20 and 300 °C with plastic deformation of about 12—13%. At the end of the tests, the samples split in the direction of compression, with the central volume fracturing and a main 45° crack forming (Fig. 15a and b). At 500 °C, the decrease in stresses upon reaching the maximum load is more uniform, and no steps are observed in the curve. Upon reaching 10% deformation, the stress increases due to
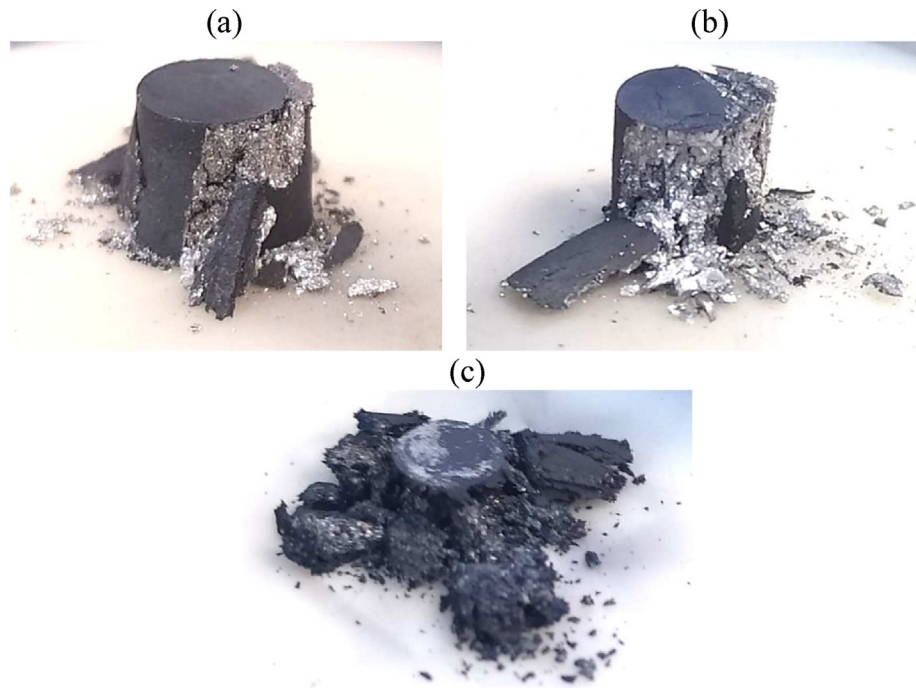
Fig. 15 — Samples of Pb—19La after compression tests at (a) 20 °C, (b) 300 °C, (c) 500 °C.
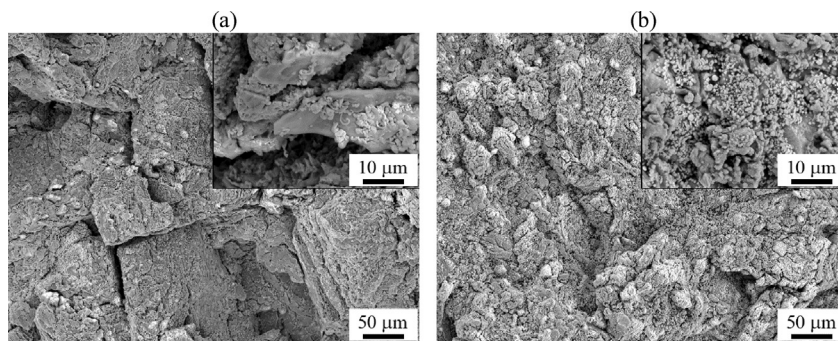

Fig. 16 — Fracture surface morphology of Pb—19La specimens after compression testing at (a) 20 °C and (b) 500 °C.

an increase in the cross-sectional area. The specimens do not completely fracture under compression at 500 °C, despite the chipping of a significant number of fragments around the central part (Fig. 15c).

Fig. 16 displays the fracture surface of specimens subjected to compression testing at 20 and 500 °C. Despite placing the specimen in oil after the test, both specimens displayed corrosion in the form of whiskers and nodules of pure lead (enlarged images in the upper right corners). Nonetheless, the difference in fracture surfaces is noticeable. At room temperature, the specimen fractured in a brittle manner with large cracks frequently oriented at 90° to each other (Fig. 16a). By contrast, the fracture surface after a compression test at 500 °C appears to be much more developed, with an evidently higher proportion of the ductile component (Fig. 16b).

Overall, the Pb—19La alloy exhibits sufficient strength for its use as a functional material in the fusion reactor breeder blanket. Although the alloy is brittle at low temperatures, the formation of cracks does not lead to rapid and complete fracture of the specimen. The compressive strength of above 110 MPa can be achieved even at 500 °C without complete fracture of the specimen.

4. Conclusions

In the framework of the R&D EUROfusion activity for the development of the DEMO breeder blankets, the Pb—19La solid neutron multiplier was produced and tested. Both argon-arc and induction melting techniques were used to cast Pb—19La ingots suitable for trial experiments. During the argon-arc melting process, the evaporation of lead caused a shift in the composition of the alloy, resulting in the formation of $LaPb_3$ and $LaPb_2$ structures with approximately equal volume fractions. On the other hand, induction melting was found to be more effective, producing a material with almost single-phase

$LaPb_3$ grains of about 80 μm in size and a small amount of $LaPb_2$ (about 3%) primarily along the grain boundaries.

Pb−19La samples are highly susceptible to corrosion when exposed to air or water. As a result of corrosion, pure lead and lanthanum hydroxide are formed, the volume of which is approximately 40% larger than that of $LaPb_3$. This leads to the formation and opening of the cracks, first along the grain boundaries, and then inside the grains. Testing the sample at 300 °C in air exhibited rapid corrosion, with the complete consumption of the sample within 20−30 h. However, corrosion at 500 °C was observed to be slower owing to the formation of pure lead as a corrosion product, which melts and can establish a layer of liquid within the corrosion layer, leading to a decelerated corrosion process. $LaPb_3$ has a hardness of 100 HV and a strength of about 193 MPa at room temperature. With an increase in temperature to 500 °C, the strength decreases to 113 MPa.

The results obtained suggest that lanthanum plumbide, $LaPb_3$, has potential for use in DEMO blanket technology as a neutron multiplier. However, its high sensitivity to corrosion in both air and water environments makes it unsuitable for direct use without additional preparation. One potential solution to this issue could be to encase the $LaPb_3$ blocks in steel, which would protect them from accidental exposure to air or water.

CRediT authorship contribution statement

R. Gaisin: Investigation, Writing - Original Draft, Writing - Review & Editing, Visualization, Methodology. **P. Pereslavtsev**: Methodology, Conceptualization, Writing&Review, S. Baumgaertner: Investigation. **K. Seemann**: Investigation. **E. Gaisina**: Investigation. **V. Chakin**: Methodology, Supervision. **S. Udartsev**: Investigation, Methodology, Funding acquisition. **P. Vladimirov**: Supervision, Conceptualization, Funding acquisition, Writing - Review & Editing. **B. Gorr**: Writing - Original Draft, Funding acquisition.

Declaration of competing interest

The authors declare that they have no known competing financial interests or personal relationships that could have appeared to influence the work reported in this paper.

Acknowledgements

REFERENCES

[1] Boccaccini LV, Arbeiter F, Arena P, Aubert J, Bühler L, Cristescu I, et al. Status of maturation of critical technologies and systemss design: breeding blanket. Fusion Eng Des 2022;179:113116. https://doi.org/10.1016/j.fusengdes.2022.113116.

[2] Fischer U, Boccaccini LV, Cismondi F, Coleman M, Day C, Hörstensmeyer Y, et al. Required, achievable and target TBR for the European DEMO. Fusion Eng Des 2020;155:111553. https://doi.org/10.1016/j.fusengdes.2020.111553.

[3] Hernández FA, Pereslavtsev P. First principles review of options for tritium breeder and neutron multiplier materials for breeding blankets in fusion reactors. Fusion Eng Des 2018;137:243−56. https://doi.org/10.1016/j.fusengdes.2018.09.014.

[4] Hernández FA, Pereslavtsev P, Zhou G, Kang Q, D'Amico S, Neuberger H, et al. Consolidated design of the HCPB breeding blanket for the pre-conceptual design phase of the EU DEMO and harmonization with the ITER HCPB TBM program. Fusion Eng Des 2020;157:111614. https://doi.org/10.1016/j.fusengdes.2020.111614.

[5] Pereslavtsev P, Fischer U, Hernandez F, Lu L. Neutronic analyses for the optimization of the advanced HCPB breeder blanket design for DEMO. Fusion Eng Des 2017;124:910−4. https://doi.org/10.1016/j.fusengdes.2017.01.028.

[6] Del Nevo A, Arena P, Caruso G, Chiovaro P, Di Maio PA, Eboli M, et al. Recent progress in developing a feasible and integrated conceptual design of the WCLL BB in EUROfusion project. Fusion Eng Des 2019;146:1805−9. https://doi.org/10.1016/j.fusengdes.2019.03.040.

[7] Walsh KA. Beryllium chemistry and processing. ASM International; 2009.

[8] Donne MD, Dorner S, Lupton DF. Fabrication and properties of Zr5 Pb3, a new neutron multiplier material for fusion blankets. J Nucl Mater 1986:369−72.

[9] Demel John Tallev. Low temperature heat capacity of YPb3, LaPb3, La5Pb3 and La5Pb3C. Retrospective Theses and Dissertations; 1973.

[10] Canepa F, Costa GA, Olcese GL. Thermodynamics and magnetic properties of LaPb3 and CePb3. Solid State Commun 1983;45:725−8. https://doi.org/10.1016/0038-1098(83)90242-9.

[11] Feyzioğlu KF, Salmankurt B, Duman S. The structural, electronic, dynamical and thermal properties of LaSn3 and LaPb3. AIP Conf Proc 2017;1815:120003. https://doi.org/10.1063/1.4976475.

[12] Jezierski A, Kaczkowski J, Cichorek T. Electronic structure and magnetic properties of La1-xCexPb3 and La1-xPrxPb3 alloys. Acta Physica Polonica A 2014;125:111−4.

[13] Ebihara T, Haga Y, Yamamoto E, Aoki Y, Sato H, Dhar SK, et al. Single crystal growth and physical properties of YbPb 3. J Phys Soc Jpn 1997;66:1842−3. https://doi.org/10.1143/JPSJ.66.1842.

[14] Liu Meng, Xian Aiping. Spontaneous growth of whiskers on RE-bearing intermetallic compounds of Sn-RE, In-RE, and Pb-RE. J Alloys Compd 2009;486:590−6.

[15] Palenzona A, Cirafici S. The la-pb (lanthanum-lead) system. J Phase Equil 1992;13:36−42. https://doi.org/10.1007/BF02645374.

[16] M. Idbenali, C. Servant, N. Selhaoui, L. Bouirden, Thermodynamic modelling of the La-Pb Binary system, JEEP − journées d'Etude des Equilibres entre Phases. https://doi.org/10.1051/jeep/200900010.

[17] Gschneidner, Jr., K.A. and Daane, A.H. (Ed.), Handbook on the physics and chemistry of rare earths, Vol. vol. 11:

Physical metallurgy Physical metallurgy. In Gschneidner, Jr., K.A. and Eyring, L. (eds.), North Holland, Amsterdam, 1988.

[18] N.K. C.K. Gupta, Extractive metallurgy of rare earths. Boca Raton: CRC Press; 2005.

[19] Love B, Kleber EV. Rare earths: sixteen new metals are ready to use. Materials in Design Eng 1960:52.

[20] Jackson RL, Crandall ER. A multiphysics coupled electro-thermo-mechanical model of whisker shorting. In: 2018 IEEE Holm Conference on Electrical Contacts; 2018. p. 48—55.

[21] Suganuma K, Baated A, Kim K-S, Hamasaki K, Nemoto N, Nakagawa T, et al. Sn whisker growth during thermal cycling. Acta Mater 2011;59:7255—67. https://doi.org/10.1016/j.actamat.2011.08.017.

[22] ASM Handbook Committee. Properties and selection: nonferrous alloys and special-purpose materials. ASM International; 1990.